35rd European Modeling & Simulation Symposium
20th International Multidisciplinary Modeling & Simulation Multiconference

2724-0029 © 2023 The Authors.
doi: 10.46354/i3m.2023.emss.019

Unit cell model of a terahertz intelligent reflecting surface with Schottky microcontacts

Anatoliy Prikhodko[1,2], Terentiy Yaropolov[1], Alexander Shurakov[1,2] and Gregory Gol'tsman[1,2]

[1]Moscow Pedagogical State University, 1/1 Malaya Pirogovskaya Str., Moscow, 119991, Russia
[2]National Research University Higher School of Economics, 20 Myasnitskaya ulitsa, Moscow, 101000, Russia

*Corresponding author. Email address: anprihodko@hse.ru

Abstract

The future of wireless networks is tightly related to the use of the terahertz frequency band. Due to the significant decrease in available power at carrier frequencies in wireless channels, the next-generation communication systems should utilize novel electronic devices for a highly directional and fast beam steering. It can be implemented if revised antenna array solutions are employed for transceiving and routing of terahertz beams. The development of time-efficient and reliable simulation techniques is vital to their designs. In this work, we report on the hybrid model of a terahertz reflective phase shifter that can be used as a unit cell in intelligent reflecting surfaces. The phase shifter is configured via biasing of built-in Schottky diodes. Explicitly defined impedance-voltage characteristics of the diodes are introduced into the parameterized electromagnetic model of the phase shifter for the Floquet port analysis. The developed model enables rigorous analysis of the intelligent reflecting surface performance beyond 100 GHz. In particular, we use it to develop requirements on planar diodes with Schottky microcontacts suitable for a 140 GHz intelligent reflecting surface with 2-bit unit cells. The modeling shows that an ideality factor of 1.5, a saturation current of 13 pA, a series resistance of 5 Ω, and an anode shunt capacitance of 3 fF are sufficient to implement such a surface with a reflectance below −2 dB.

Keywords: Terahertz; intelligent reflecting surface; Schottky diode; Lambert W function; Floquet port analysis

1. Introduction

Society needs in information handling capacity inevitably grow. This motivates active studies in the next-generation communication area (Giordani et al., 2020). The terahertz (THz) frequency band is considered beneficial for the upcoming sixth-generation (6G) wireless networks. Its utilization, however, is accompanied by the necessity to deal with high propagation losses due to atmospheric absorption, scattering on obstacles and dynamic blockages (Shurakov et al., 2023). Thus, 6G wireless systems should rely on THz transmitters and receivers with highly directive reconfigurable beams. This together with the use of intelligent reflecting surfaces (IRSs) is proposed as a promising solution for the enhanced signal delivery at carrier frequencies beyond 100 GHz (Basar et al., 2019).

Generally speaking, IRS consists of numerous periodic elements providing effective control of the wavefront altering the phase, magnitude and polarization upon beam routing (Long et al., 2021). A large number of IRS designs is recently proposed. Those include devices with tuning mechanisms based on i) slow-speed liquid crystals and micro electromechanical systems, ii) ultrafast transistor and diode-based electronics (Yang et al., 2022).

Considering a practical IRS as a part of a sub-THz wireless channel, one needs to account for the phase-dependent amplitude response of its unit cells, as well

as for the cross-coupling between them (Jian et al., 2022). Beamforming optimization can be performed either i) analytically, using an equivalent circuit model of a generalized IRS structure (Abeywickrama et al., 2020), or ii) numerically, upon electromagnetic (EM) modeling (Costa and Borgese, 2021). The majority of recently reported IRS models, however, focuses on operating frequencies well below 100 GHz, when discrete metal-oxide-semiconductor field-effect transistors (MOSFETs) and varactor or positive-intrinsic-negative (PIN) diodes can be used for phase shifting (Liu et al., 2019; Zhu et al., 2013; Dai et al., 2020). This results in a variety of unconsidered aspects related to the development and implementation of a THz IRS as a monolithic integrated circuit (IC). Moreover, the existing unit cell models of IRS are rather indirectly linked to semiconductor physics. And they do not allow one to easily predict changes in performance at different incident power levels due to temperature-dependent transport properties of space charge regions in IRS unit cells (Tang et al., 2012; Tarasova et al., 2021).

The use of Schottky diodes in an IRS unit cell ensures its state switching time of less than a picosecond (Vassos et al., 2021). Given the fundamental lack of charge carriers inertia, performance of a Schottky diode is completely determined by fabrication technology (Mehdi et al., 2017) and EM design of its IC (Tang et al., 2013). Thus, the appearance of time-efficient and reliable simulation techniques is vital to further progress of the THz Schottky diode technology.

In this work, we report on the hybrid model of a THz reflective phase shifter that can be used as an IRS unit cell. The phase shifter is configured via biasing of built-in Schottky diodes. Explicitly defined impedance-voltage characteristics of the diodes are introduced into the parameterized EM model of the phase shifter for the Floquet port analysis. The developed model is used for the IRS performance simulations at 140 GHz.

The paper describes the methodology and main results of our study as follows. Section 2.1 is focused on the analytic modeling of transport properties of microscale Schottky contacts suitable for THz applications. Section 2.2 provides the extraction procedure of geometry-dependent parasitic parameters of planar diodes with Schottky microcontacts. Parameterized EM model of a THz reflective phase shifter making use of Schottky diode switches for phase control is described in section 2.3. The main findings are further summarized in the conclusion section.

2. Methodology and Main Results

In this section, we focus on the modeling of a 140 GHz uniform IRS making use of revised planar patch antenna array. Each IRS unit cell utilizes metallic slotted screen with microscale Schottky diodes. When biasing them, one changes the phase shift upon reflection of an EM wave. Magnitude and phase of the reflection coefficient are acquired by the Floquet port analysis. The diodes are consequently modeled as full-scale multilayer systems and their RLC-circuits with predefined nonlinear properties. To ensure feasibility of further IRS fabrication, we rely on the Schottky diodes actually produced in our cleanroom.

2.1. Microscale Schottky Contact

Equation 1 is used to explicitly define current-voltage characteristic of a Schottky diode, $I_d(V_d)$, by the Lambert W_0 function (Jung and Guziewicz, 2009; Prikhodko et al., 2021). We use this function to extract direct current (DC) transport parameters for a series of GaAs Schottky diodes fabricated at our cleanroom facility. The diodes utilize Schottky contacts with area $A = 0.785\ \mu m^2$ and dopant concentration in n-GaAs epi-layer $N_d = 4.2 \times 10^{17}\ cm^{-3}$.

$$I_d(V_b) = \frac{\eta V_t}{R_s} W_0\left(\frac{I_s R_s}{\eta V_t}\exp\left(\frac{V_b + I_s R_s}{\eta V_t}\right)\right) - I_s, \qquad (1)$$

where η is the ideality factor, I_s is the saturation current, R_s is the series resistance and V_t is the thermal voltage. Mean and standard deviation values of the extracted DC parameters are provided in table 1.

Table 1. DC transport parameters of the fabricated Schottky diodes extracted via W_0-fitting.

$\bar{\eta}$	σ_η	$\bar{I}_s$ [pA]	σ_{I_s} [pA]	$\bar{R}_s$ [Ω]	σ_{R_s} [Ω]
1.51	0.08	12.6	8.38	4.98	2.01

To properly implement THz Schottky diode IC, it is also vital to account for the alternating current (AC) transport properties of a Schottky contact. In case of conventional RC-model, the equivalent circuit of the space charge region is presented by the voltage-dependent resistance $R_j(V_b)$ and capacitance $C_j(V_b)$ connected in parallel. And one can define its differential conductivity as $dG_j(V_b) = dI_j(V_b)/dV_b$, where I_j is the transport current through the Schottky barrier in accordance with the thermionic emission model (Sze et al., 2021). When minor impact of the time-varying depletion region width is neglected for small signals, the impedance of the Schottky contact, $\hat{Z}_j(V_b)$, obeys equation 2 for a given operating frequency, f.

$$dG_j(V_b) = \frac{d}{dV_b}\left(\bar{I}_s \exp\left(\frac{V_b}{\bar{\eta} V_t}\right) - \bar{I}_s\right)$$
$$C_j(V_b) = A\left(\frac{2(\psi_{bi} - V_b)}{\varepsilon_r \varepsilon_0 q N_d}\right)^{-0.5}, \text{where}$$
$$\psi_{bi} = \bar{\eta} V_t \ln\left(\frac{A A_R T^2}{\bar{I}_s}\right) - (\bar{\eta} - 2) V_t \ln\left(\frac{N_c}{N_d}\right),$$

where ε_r is the relative permittivity of GaAs, ε_0 is the vacuum permittivity, q is the electronic charge, A_R is the Richardson constant, N_c is the temperature-dependent density of states in the conduction band and T is the oper-

ating temperature.

$$\hat{Z}_j(V_b) = \left(dG_j(V_b) + i\,2\pi f\,C_j(V_b)\right)^{-1} \tag{2}$$

2.2. Planar Schottky Diode

For series interconnection of a two-port lumped circuit with impedance $\hat{Z}_{RLC}$ and input/output lossless transmission lines with impedances $\hat{Z}_0$ and electrical lengths ϕ, the resulting ABCD-parameters matrix is defined by equation 3. Equations 4–6 determine the ABCD-parameters matrices of the input transmission line, the lumped circuit and the output transmission line, respectively.

$$ABCD_{res} = \prod_{m=1}^{3} ABCD_m, \text{ where} \tag{3}$$

$$ABCD_1 = \begin{bmatrix} \cosh(i\phi) & \hat{Z}_0 \sinh(i\phi) \\ \hat{Z}_0^{-1} \sinh(i\phi) & \cosh(i\phi) \end{bmatrix} \tag{4}$$

$$ABCD_2 = \begin{bmatrix} 1 & \hat{Z}_{RLC} \\ 0 & 1 \end{bmatrix} \tag{5}$$

$$ABCD_3 = \begin{bmatrix} \cosh(i\phi) & \hat{Z}_0 \sinh(i\phi) \\ \hat{Z}_0^{-1} \sinh(i\phi) & \cosh(i\phi) \end{bmatrix} \tag{6}$$

As shown in figure 1, we choose a coaxial transmission line to probe impedance of a planar Schottky diode. We use HFSS as a simulation software. The transmission line is excited by two wave ports (Port 1 and Port 2). Both planar inner wire and surrounding concentric shield (GND) of the transmission line are modeled as perfect conductors. The inner volume is filled with vacuum. The Schottky diode is integrated with the planar wire. The wire, in turn, is surrounded by quartz and polyethylene substrates with permittivities $\varepsilon_{r1} = 3.78$ and $\varepsilon_{r2} = 2.25$, respectively. We use a symmetry plane (SP) boundary to increase accuracy for a given simulation time. Geometrical parameters of the transmission line and the diode are summarized in table 2. The developed EM model has an equivalent circuit provided in figure 2.

We adjust the developed EM model in accordance with figure 1(b) and calculate the resulting Y-parameters matrix. Given that Schottky contact is implemented by the anode suspended bridge contacting GaAs mesa, the bridge impedance $\hat{Z}_b = (i\,2\pi f\,C_b - i\,(2\pi f\,L_b)^{-1})^{-1}$ can be directly extracted. We model all the structural elements of the diode IC, except for the SiO_2 layer, as perfect conductors. Thus, only the imaginary part of the admittance is of interest. Since $\phi \approx 0$ for the chosen transmission line length, the interrelation between Y- and ABCD-parameters defined by equation 7 can be reduced to equation 8. Since $\hat{Z}_{RLC} = \hat{Z}_b$ for the considered SHORT circuited planar diode structure, the calculated $Y_{res}[1,2] = 0.0571i$ S results in $\hat{Z}_b = 17.5i\ \Omega$.

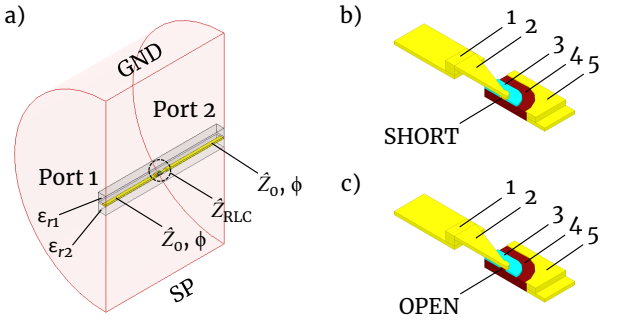

Figure 1. a) EM model of a planar Schottky diode integrated with coaxial transmission line. b–c) Planar diode structures with SHORT and OPEN circuited Schottky contacts. The notations are: 1 – anode pad, 2 – anode suspended bridge, 3 – SiO_2 layer, 4 – GaAs mesa, 5 – ohmic contact.

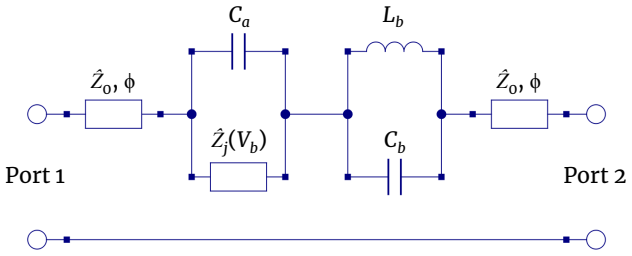

Figure 2. Equivalent circuit of a planar Schottky diode integrated with coaxial transmission line.

$$Y_{res} = \frac{1}{ABCD_{res}[1,2]} \begin{bmatrix} ABCD_{res}[2,2] & -|ABCD_{res}| \\ -1 & ABCD_{res}[1,1] \end{bmatrix} \tag{7}$$

$$Y_{res} = \begin{bmatrix} \hat{Z}_{RLC}^{-1} & -\hat{Z}_{RLC}^{-1} \\ -\hat{Z}_{RLC}^{-1} & \hat{Z}_{RLC}^{-1} \end{bmatrix} \tag{8}$$

We further adjust the EM model in accordance with figure 1(c) and calculate the resulting Y-parameters matrix again. In this case, $\hat{Z}_{RLC} = \hat{Z}_b - i\,(2\pi f\,C_a)^{-1}$, where $f = 140$ GHz. We acquire $Y_{res}[1,2] = -0.00247i$ S, which corresponds to the anode shunt capacitance $C_a = 2.69\ fF$.

It is worth mentioning that almost identical simulation results are obtained in case of a half-wave long transmission line, i.e., when $\phi = \pi$ and equation 8 is also valid.

2.3. IRS unit cell

We use the results described earlier in sections 2.1–2.2 to explicitly define impedance-voltage characteristic, $\hat{Z}_d(V_b)$, of our typical planar Schottky diode. Equation 9 determines $\hat{Z}_d(V_b)$ for predefined $\hat{Z}_j(V_b)$, C_a, $\hat{Z}_b$. The impedance real, $Re(\hat{Z}_d)$, and imaginary, $Im(\hat{Z}_d)$, parts are plotted in figure 3 for bias voltages from -3 to 1 V. We further introduce the acquired impedance-voltage characteristic into a

Table 2. Geometrical parameters of the developed EM model.

Coaxial transmission line:							Planar Schottky diode:												
d_{out}	w_{in}	l_{tl}	h_1	w_1	h_2	w_2	h_p	w_p	t_b	w_{b1}	w_{b2}	l_b	t_d	s_d	h_m	w_m	l_m	t_c	w_c	l_c
245	10	25	10	20	10	20	1.95	10	0.5	7	1	7.5	0.25	1.5	1.2	10	7	0.1	10	7

Here d_{out} is the diameter of the transmission line shield, w_{in} is the width of the transmission line planar inner wire, l_{tl} is the transmission line total length, h_1 is the height of the quartz substrate, w_1 is the width of the quartz substrate, h_2 is the height of the polyethylene substrate, w_2 is the width of the polyethylene substrate, h_p is the height of the anode pad, w_p is the width of the anode pad, t_b is the thickness of the anode suspended bridge, w_{b1} is the width of the anode suspended bridge at anode pad, w_{b2} is the width of the anode suspended bridge at Schottky contact, l_b is the lenght of the anode suspended bridge, t_d is the SiO_2 thickness, s_d is the spacing between SiO_2 and ohmic contact, h_m is the height of the GaAs mesa, w_m is the width of the GaAs mesa, l_m is the length of the GaAs mesa, t_c is the thickness of the ohmic contact, w_c is the width of the ohmic contact, l_c is the length of the ohmic contact. All dimensions are in micrometers.

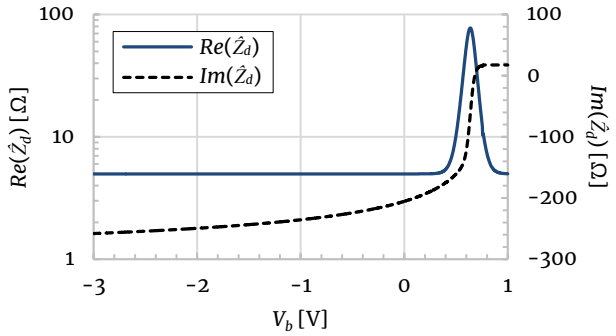

Figure 3. Impedance-voltage characteristic of our typical planar Schottky diode.

parameterized EM model of a 140 GHz IRS unit cell.

$$\hat{Z}_d(V_b) = (\hat{Z}_j(V_b)^{-1} + i\,2\pi f\,C_a)^{-1} + \hat{Z}_b \qquad (9)$$

The developed EM model of the IRS unit cell is presented in figure 4. The unit cell has half-wave dimensions. It utilizes metallic slotted screen with 5 planar Schottky diodes (PSD 0 – PSD 4) inserted in between of front and rear metallizations of a rectangular patch antenna. When biasing them, one changes the phase shift upon reflection of an EM wave. The diodes are modeled as sheet impedance boundaries for 2 different bias states. In state 0, PSD 0 has impedance $\hat{Z}_d(V_{b1})$ and PSD 1–4 have impedance $\hat{Z}_d(V_b)$. In state 1, PSD 0 and PSD 2–4 have impedance $\hat{Z}_d(V_{b1})$, PSD 1 has impedance $\hat{Z}_d(V_b)$. During simulations, we keep V_{b1} = 1 V and sweep V_b from -3 to 0.7 V. Magnitude and phase of the reflection coefficient are acquired by the Floquet port analysis. We define side faces surrounding the patch antenna and a quarter-wave vacuum insert above it as master/slave boundaries (MB 1/SB 1 and MB 2/SB 2) to implement 2-dimensional periodicity. All the metallic surfaces are modeled as perfect conductors. The width of the slots in the metallic slotted screen is 25.5 μm. Dielectric quartz (ε_{r1}) and polyethylene (ε_{r2}) substrates have thicknesses of 150 and 100 μm, respectively.

Results of the Floquet port analysis are summarized in figure 5. Here the phase shift is defined as the difference in arg($S[1,1]$) values between IRS unit cell states 0 and 1, and the reflectance is calculated as mag($S[1,1]$) mean. Maximum reflectance and nearly 90 deg phase shifts are

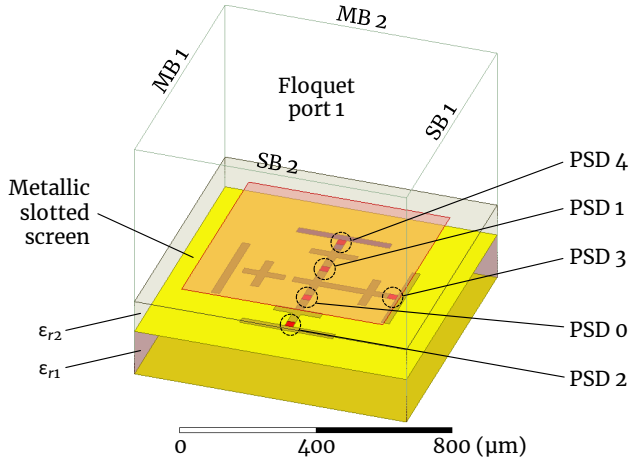

Figure 4. Parameterized EM model of a 140 GHz IRS unit cell. All linear dimensions are to scale.

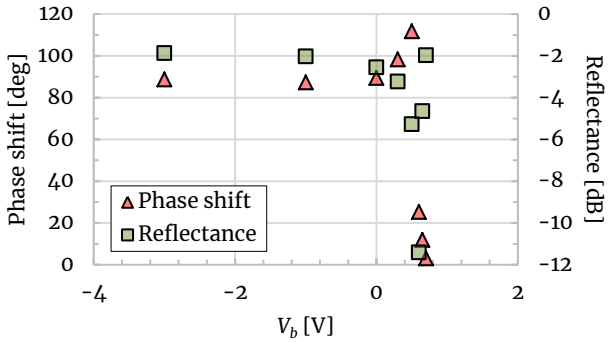

Figure 5. Results of the Floquet port analysis of a 140 GHz IRS unit cell.

observed for switching above-the-barrier DC bias voltage to that on the reverse branch of the current-voltage characteristic. This proves efficient switch-like operation of Schottky diodes and, therefore, 2-bit phase shift resolution (2 more bias states are available for a given V_b value) of IRS unit cell. Thus, the developed IRS with phase-configured unit cells (Nayeri et al., 2018) is capable of fast multi-state beam steering at 140 GHz. The forward bias voltages are characterized by either high reflection losses or constant phase shifts which is unacceptable for IRS operation. However, we believe that this can be changed, and impedance control can provide additional phase shift

states if the Schottky diodes DC and AC transport properties are properly tuned. This, in turn, should increase number of available states for IRS upon beam steering. We plan detailed investigation of this statement in the nearest future. It is also worth mentioning that the performed simulations prove the suitability of our Schottky diodes with an ideality factor of 1.51, a saturation current of 12.6 pA, a series resistance of 4.98 Ω, and an anode shunt capacitance of 2.69 fF for IRS unit cells with a reflectance of −1.8 dB. Thus, we further plan to implement a 2-bit 140 GHz IRS and to justify its simulated performance experimentally.

3. Conclusions

In this work, we focus on the modeling of a 140 GHz intelligent reflecting surface making use of revised planar patch antenna array. Each unit cell of the surface utilizes metallic slotted screen with microscale Schottky diodes. When switching their impedances, one changes the phase shift upon reflection of an electromagnetic wave. Magnitude and phase of the reflection coefficient are acquired by the Floquet port analysis. The diodes are modeled as RLC-circuits with predefined nonlinear properties. Both fundamental and implementation-dependent transport parameters of the diodes are incorporated into the developed electromagnetic model of the intelligent reflecting surface unit cell. We believe that our findings will be useful in the design optimization of such surfaces being actively developed for an ultrafast beam steering in the next-generation wireless communication systems. In particular, we assess our Schottky diode technology and find out that planar diodes with feasible parameters (namely, ideality factor of 1.5, saturation current of 13 pA, series resistance of 5 Ω, anode shunt capacitance of 3 fF) are suitable for relative phase shifts of 90 deg with corresponding reflectances below −2 dB. Thus, the fabrication and performance tests of a 140 GHz diode-based intelligent reflecting surface are in our future plans.

4. Funding

The study was supported by the Russian Science Foundation grant No. 22-79-10279, https://rscf.ru/project/22-79-10279/.

References

Abeywickrama, S., Zhang, R., Wu, Q., and Yuen, C. (2020). Intelligent reflecting surface: Practical phase shift model and beamforming optimization. *IEEE Transactions on Communications*, 68(9):5849–5863.

Basar, E., Di Renzo, M., De Rosny, J., Debbah, M., Alouini, M.-S., and Zhang, R. (2019). Wireless communications through reconfigurable intelligent surfaces. *IEEE Access*, 7:116753–116773.

Costa, F. and Borgese, M. (2021). Electromagnetic model of reflective intelligent surfaces. *IEEE Open Journal of the Communications Society*, 2:1577–1589.

Dai, L., Wang, B., Wang, M., Yang, X., Tan, J., Bi, S., Xu, S., Yang, F., Chen, Z., Di Renzo, M., et al. (2020). Reconfigurable intelligent surface-based wireless communications: Antenna design, prototyping, and experimental results. *IEEE access*, 8:45913–45923.

Giordani, M., Polese, M., Mezzavilla, M., Rangan, S., and Zorzi, M. (2020). Toward 6G networks: Use cases and technologies. *IEEE Communications Magazine*, 58(3):55–61.

Jian, M., Alexandropoulos, G. C., Basar, E., Huang, C., Liu, R., Liu, Y., and Yuen, C. (2022). Reconfigurable intelligent surfaces for wireless communications: Overview of hardware designs, channel models, and estimation techniques. *Intelligent and Converged Networks*, 3(1):1–32.

Jung, W. and Guziewicz, M. (2009). Schottky diode parameters extraction using Lambert W function. *Materials Science and Engineering: B*, 165(1-2):57–59.

Liu, F., Tsilipakos, O., Pitilakis, A., Tasolamprou, A. C., Mirmoosa, M. S., Kantartzis, N. V., Kwon, D.-H., Georgiou, J., Kossifos, K., Antoniades, M. A., et al. (2019). Intelligent metasurfaces with continuously tunable local surface impedance for multiple reconfigurable functions. *Physical Review Applied*, 11(4):044024.

Long, W., Chen, R., Moretti, M., Zhang, W., and Li, J. (2021). A promising technology for 6G wireless networks: Intelligent reflecting surface. *Journal of Communications and Information Networks*, 6(1):1–16.

Mehdi, I., Siles, J. V., Lee, C., and Schlecht, E. (2017). THz diode technology: Status, prospects, and applications. *Proceedings of the IEEE*, 105(6):990–1007.

Nayeri, P., Yang, F., and Elsherbeni, A. Z. (2018). *Reflectarray antennas: theory, designs, and applications*. John Wiley & Sons.

Prikhodko, A., Belikov, I., Mikhailov, D., Shurakov, A., and Goltsman, G. (2021). Towards multipixel THz Schottky diode detector with a single RF output line. *Journal of Physics: Conference Series*, 2086(1):012063.

Shurakov, A., Moltchanov, D., Prikhodko, A., Khakimov, A., Mokrov, E., Begishev, V., Belikov, I., Koucheryavy, Y., and Gol'tsman, G. (2023). Empirical blockage characterization and detection in indoor sub-THz communications. *Computer Communications*, 201:48–58.

Sze, S. M., Li, Y., and Ng, K. K. (2021). *Physics of semiconductor devices*. John Wiley & Sons.

Tang, A. Y., Drakinskiy, V., Yhland, K., Stenarson, J., Bryllert, T., and Stake, J. (2013). Analytical extraction of a Schottky diode model from broadband S-parameters. *IEEE transactions on microwave theory and techniques*, 61(5):1870–1878.

Tang, A. Y., Schlecht, E., Lin, R., Chattopadhyay, G., Lee, C., Gill, J., Mehdi, I., and Stake, J. (2012). Electrothermal model for multi-anode schottky diode multipliers. *IEEE Transactions on Terahertz Science and Technology*, 2(3):290–298.

Tarasova, E., Puzanov, A., Bibikova, V., Volkova, E., Zabavichev, I. Y., Obolenskaya, E., Potekhin, A., and Obolensky, S. (2021). The physical topological modeling of single radiation effects in submicron ultrahigh-frequency semiconductor diode structures with taking in account the heating of an electron-hole gas in the charged particle track. *Proceedings of the 33rd European Modeling Simulation Symposium (EMSS 2021)*, pages 289–294.

Vassos, E., Churm, J., Powell, J., Viegas, C., Alderman, B., and Feresidis, A. (2021). Air-bridged Schottky diodes for dynamically tunable millimeter-wave metamaterial phase shifters. *Scientific Reports*, 11(1):5988.

Yang, F., Pitchappa, P., and Wang, N. (2022). Terahertz reconfigurable intelligent surfaces (RISs) for 6G communication links. *Micromachines*, 13(2).

Zhu, B. O., Zhao, J., and Feng, Y. (2013). Active impedance metasurface with full 360 reflection phase tuning. *Scientific reports*, 3(1):3059.